Supporting Information

Near Infrared-Triggered Photodynamic, Photothermal and On-Demand Chemotherapy by Multifunctional Upconversion Nanocomposite

Balmiki Kumar, [†] *Aparna Murali,* [‡] *Irshad Mattan,* [†] *and Supratim Giri*[*†]

[†]*Department of Chemistry, National Institute of Technology, Rourkela. Odisha- 769008, India*

**E-mail: girisupr@nitrkl.ac.in*

[‡]*Department of Biotechnology and Medical Engineering, National Institute of Technology, Rourkela. Odisha- 769008, India*

1. **Materials.**

Yttrium oxide (Y_2O_3, 99.99%), ytterbium oxide (Yb_2O_3, 99.99%), thulium oxide (Tm_2O_3, 99.99%), erbium oxide (Er_2O_3, 99.99%) oleic acid (OA, 90%), 1-octadecene (ODE, 90%), trifluoroacetate (TFA, 99%), sodium trifluoroacetate ($NaCOOCF_3$, 98%), anhydrous ferric chloride, chloroauric acid, silver nitrate, n-cetyltrimethylammonium bromide (CTAB), tetraethylorthosilicate (TEOS), tetrabutyltitanate (TOBT), 1-ethyl-3-(3-dimethylaminopropyl)carbodiimide (EDC.HCl), lithium chloride, 3-aminopropyltriethoxysilane (3-APTES), 1,3-diphenylisobenzofuran (DPBF) and bovine serum albumin (BSA) were purchased from Sigma-Aldrich, India. Folic acid (FA), anhydrous dimethylsulfoxide (DMSO), N-hydroxysuccinimide (NHS), ruthenium (III) chloride trihydrate ($RuCl_3.3H_2O$), 1,10-phenanthroline, perchloric acid, sodium borohydride, chloroform, pyridine, acetonitrile and ammonia solution (NH_3, 25%), fluorosceinisothiocyanate (FITC), Rhodamine B dye along with the other chemicals for phosphate buffers were obtained from Hi-Media Pvt. Ltd., Mumbai, India. All the chemicals used were of analytical grade and used for the various steps without further purification. Deionized (DI) water (Millipore Co., USA; 18.2 MΩ.cm resistivity at 25°C) was used throughout the experiments. Human Cervical adenocarcinoma (HeLa) cell line was procured from NCCS Pune, India.

2. **Methods**

a. Colloidal stability and protein binding assay.

The stability of nanoconjugates (CSUT-MS, CSUT-MSDG and CSUT-MSDGG) in different media (DI water, PBS buffer and DMEM media with 10 % FBS) was determined by dynamic light scattering (DLS) measurement. Briefly, 1.0 mg of nanoconjugates were added to 2.0 ml of each of the abovementioned dispersion media. The dispersion was sonicated well for 15 mins to disaggregate the particles. At first, the DLS measurement of freshly dispersed

suspension was carried out. Next, the dispersions were left undisturbed for 6 h and subjected to DLS measurements after a gentle tap to the dispersions. Zeta-potential studies of the nanoconjugates were carried out in PBS buffer (pH 7.4).

Protein binding assay was carried out as follows: In a typical protocol, 5.0 mg of CSUT-MS, CSUT-MSDG and CSUT-MSDGG, were dispersed in 500 µl of BSA solution (2.0 mg/ml, in PBS buffer), the mixture was stirred for 2 h at room temperature. The nanoconjugates were separated from the protein solution by centrifugation. The supernatant was collected analysed for the change in concentration by standard Bradford's assay using UV-vis analysis at 595 nm. The change in the BSA concentration due to interactions with the nanoconjugates was calculated using following equation: loading (%) = $(C_I - C_F)/C_F \times 100\%$ where, C_I is the initial amount of BSA taken for loading and C_F is the final concentration after loading experiment.

2.2. *In-vitro* studies of NIR triggered multimodal therapeutic effects on HeLa cells.

2.2.1. Cytocompatibility studies through MTT assay. Human cervical adenocarcinoma (HeLa) cells were cultured in Dulbecco's Modified Eagle's medium (DMEM) supplemented with 10% FBS in a CO_2 incubator (37ºC, 5% CO_2, 95% humidity). To check the cytocompatibility of each set, i.e., CSUT-MS and CSUT-MSDG and CSUT-MSDGG, on cancer cells, the HeLa cells were seeded at an initial cell seeding density of $3x10^3$ cells/well in the culture medium onto 96-well plate. The CSUT-MS and CSUT-MSDG and CSUT-MSDGG were added to the cells at different concentrations ranging from 25-200 µg/mL in triplicates for each concentration (25, 50, 100 and 200 µg/mL). Cell viability was measured following the standard MTT (Himedia EZCount MTT Assay Kit CCK-003) protocol.

2.2.2. FITC tagging of nanoconjugate for tracking intracellular localizations. The nanoconjugates were tagged with FITC (fluorescein isothiocyanate) using a previously reported method with a slight modifications.[1] 10 mg of nanoparticles were suspended in 1 ml ethanolic solution of 250 µg/ml FITC (1 mg/ml). The mixture was allowed to stir overnight in

dark conditions at room temperature. The final product was then washed multiple times with distilled water to remove any trace of physisorbed FITC from the surface.

To track the intracellular localization of FITC tagged nanoplatform, the HeLa cells seeded on a coverslip and treated with particles were incubated for 12 h. Prior to the observation, the cells were washed with PBS buffer to remove any unbound particles. Subsequently, the particle treated cells were observed under the confocal microscope.

2.2.3. Rhodamine B (RhB) tagging of CSUT-MS and FITC tagged BSA coated GNR for nanoplatform integrity studies. Briefly, 3 ml aqueous solution 2 mg of RhB, 2 mg of EDC.HCl and 5 mg of NHS was stirred for 1 h in dark to activate the carboxyl group in RhB. Subsequently, 10 mg of aqueous dispersion of CSUT-MS in 1 ml DI water was added to the activated RhB solution. The mixture was stirred for 8 h at r.t. in dark conditions. The RhB tagged product was washed repeatedly with ethanol-water mixture to remove all the physisorbed molecules of RhB.

Next, to synthesise FITC tagged BSA coated GNRs, 16 mg of BSA dispersed in DMSO (2 ml) was mixed with 100 µl of FITC solution (1 mg/ml), the mixture was stirred for 6 h at r.t. in dark conditions to obtain FITC tagged BSA. A thoroughly washed GNR sample was then mixed with 1 ml solution of FITC-BSA and the content was stirred for overnight at r.t. while maintaining the dark conditions. The excess of FITC was washed by repeated centrifugation and re-dispersion with DI water. Finally, the RhB and FITC tagged nanoplatform was synthesised by adding 1 ml of FITC-tagged BSA modified GNR (FITC-BSA-GNR) to RhB modified CSUT-MS. The mixture was stirred for 6 h to obtain the nanoplatform with RhB tagged CSUT-MS and FITC tagged GNRs. The confocal study was carried out by the protocol similar to described in previous section (2.2.2).

2.2.4. Intracellular ROS detection by flow cytometry studies. To analyze the ROS generation capacity of each set (*i.e.*, CSUT-MS and CSUT-MSDG and CSUT-MSDGG) in the cells, flow cytometry based oxidative stress detection using DCFDA dye was performed

by following the instructor's manual (Abcam ab139476). Briefly, HeLa cells were seeded at an initial cell density of $1X10^5$ cells/well in a 6-well plate. After adhesion, cells were incubated with the particles from each set at a concentration of 50 µg/mL. After an overnight incubation, the cells were collected by trypsinization and washed with 1X ROS washing buffer. The cells were re-suspended in the oxidative stress detection dye solution (1:1000 dilutions with 1X ROS washing buffer). The cell suspension was then subjected to irradiation with NIR for 20 min with 1 min intervals for every 5 minutes of irradiation. Soon after the exposure, the cells were analyzed through flow cytometry (FACS Accuri C6, BD Biosciences). For better understanding of the event, data corresponding to 10 min exposure was reported.

2.2.5. Trypan blue dye exclusion based live-dead assay. To study the therapeutic effects of the groups in response to NIR irradiation, the concentration of 50 µg/mL was chosen based on the cytocompatibility data for all the subsequent cell studies.

For NIR irradiation-based experiments, HeLa cells were seeded ta an initial cell density 1.5 x 10^5 cells/well onto a 6 well plate. The cells were incubated with the nanoparticles from each set (CSUT-MS and CSUT-MSDG and CSUT-MSDGG) overnight to facilitate their uptake. The cells were then washed twice with PBS to remove any unbound particles from the cell surface. The cells were collected by trypsinization and transferred into 1.5 ml centrifuge tube, pelleted down by centrifugation and the pellet was irradiated with NIR laser at a power density of 0.7 W/cm^2. After 20 min of exposure (cycle of 5 min exposure and 1 min gap), the cells were incubated for an additional 48 h. Finally, the cells were trypsinized and washed with DPBS. Subsequently, equal volume of trypan blue dye solution was added to cell suspension and live cells were counted manually using haemocytometer under a phase-contrast microscope (Primovert, Carl Zeiss, Germany).

2.2.6. Propidium iodide (PI) based live-dead assay by flow cytometry. Post NIR treatment according to the method already described above (sec. 2.1.5), the cells were subjected to

trypsinization, collected and washed twice with ice-cold DPBS. Both live and dead cells were then stained with 500 µL of PI (50 µg/mL in DPBS) for 20 min at room temperature in dark conditions. Live-dead assay was performed by analyzing the sample on a flow cytometer (C6 Accuri BD Bioscience, USA).

Additionally, to categorically distinguish the therapeutic contribution from each of the therapeutic component (i.e., only PDT, only chemo and only PTT) present separately in the monomodal modifications of the nanoplatforms were evaluated after NIR exposure experiments by PI based live-dead assay using protocol discussed above.

2.2.7. Flow cytometry-based apoptosis assay. The protocol for the incubation of the HeLa cells with the nanoparticles was performed according to the method described in Sec 2.2.4. After the exposure of the cell suspension with the IR radiation, the cells were re-plated and incubated for 24 h. The apoptotic and necrotic cells population was analyzed using apoptosis assay kit (BD Pharmingen, 559763) following the manufacture's instruction. Annexin V (AV) was used for the detection of early apoptotic cells and 7-Aminoactinomysin (7AAD) was used for the detection of necrotic cells. The trypsinized cells were stained with the dyes (1:100 dilutions with 1X binding buffer). After incubation for 15 min in the dark, the cells were analyzed through flow cytometry.

2.2.8. Intracellular ROS detection through confocal studies. The HeLa cells were visualized under a confocal microscope (Leica TCS SP8, Germany) to determine the ROS generation in the presence of 50 µg/mL of particles. Previously mentioned procedure was followed for the loading of the nanoparticles onto the cells. Prior to the observation, the cells were washed with the 1X ROS washing buffer. Then the particle treated cells were irradiated for 5 min in the presence of the ROS detection dye and immediately observed under the confocal microscope.

2.2.9. Confocal studies on cytoskeletal organization of HeLa cells post NIR irradiation. To observe the morphology of the HeLa cells, post NIR irradiation, particle treated cells were

fixed with 4% paraformaldehyde after 24 h of incubation. The cell's cytoskeletal F-actin filaments were stained with TRITC-Phalloidin (50 µg/mL) and the nucleus was stained with Hoechst (5 µg/mL) The stained cells were then analyzed by confocal microscopy (Leica TCS SP8, Germany).

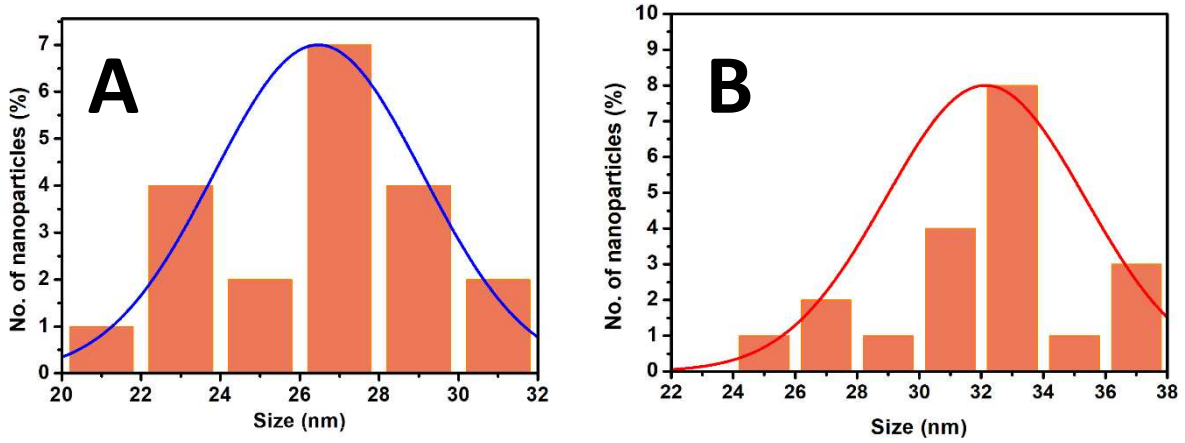

Fig. S1. Histogram showing the size distribution of core and core-shell upconversion (CSU) nanoparticles analyzed from TEM analysis.

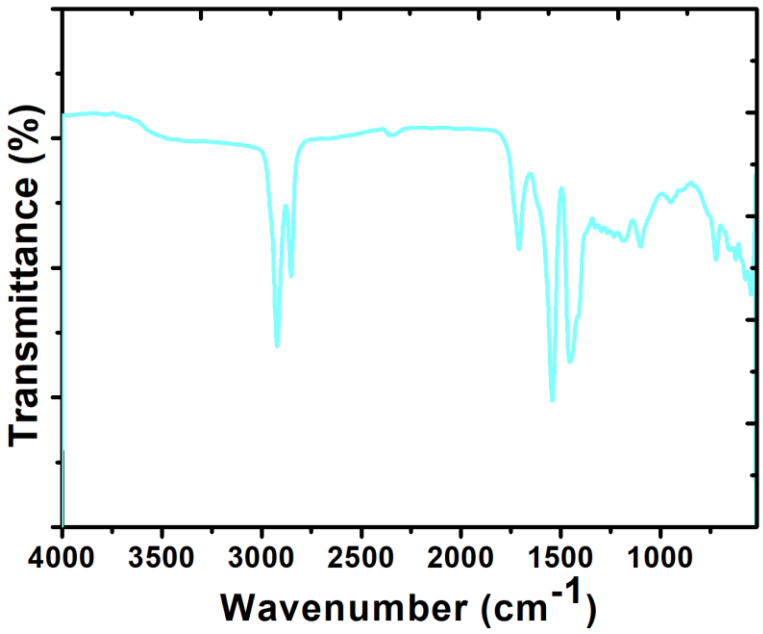

Fig. S2. FTIR spectrum of oleic acid capped core-shell upconversion (CSU) nanoparticles.

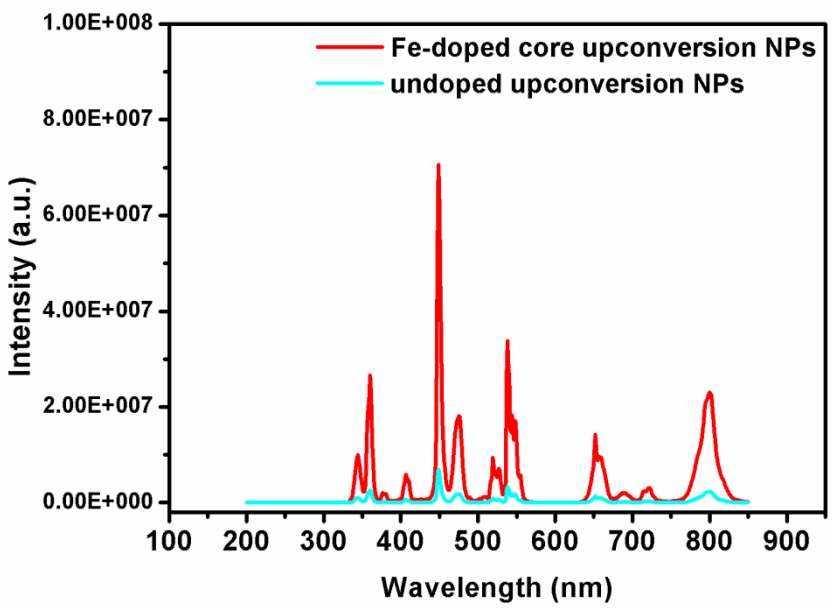

Fig. S3. Fluorescence analysis of un-doped core (blue curve) and 20 % Fe-doped core upconversion nanoparticles (red curve).

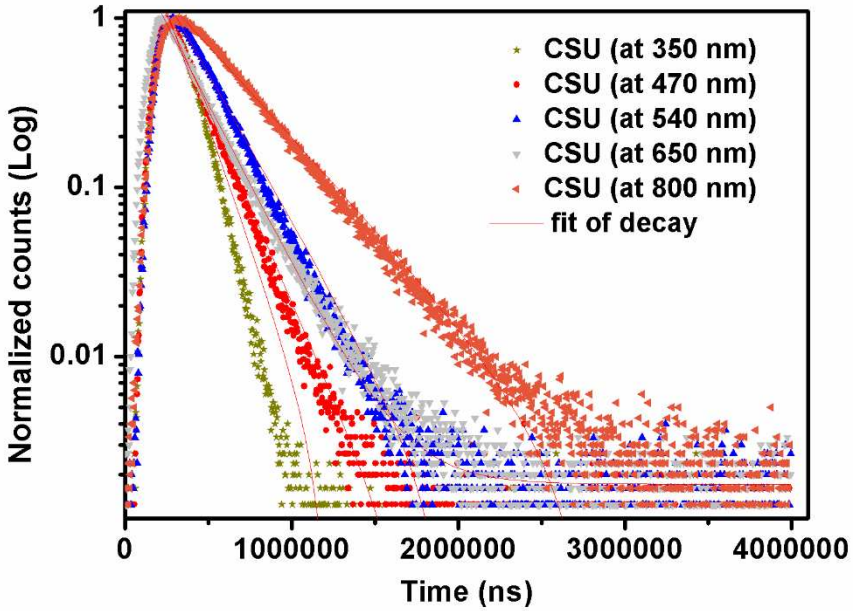

Fig. S4. Fluorescence lifetime studies of Fe^{3+}-ion doped core upconversion nanoparticles at various emissions, i.e. 350 nm (0.15 ms), 470 nm (0.19 ms), 540 nm (0.25 ms), 650 nm (0.22 ms) and 800 nm (0.40 ms), respectively.

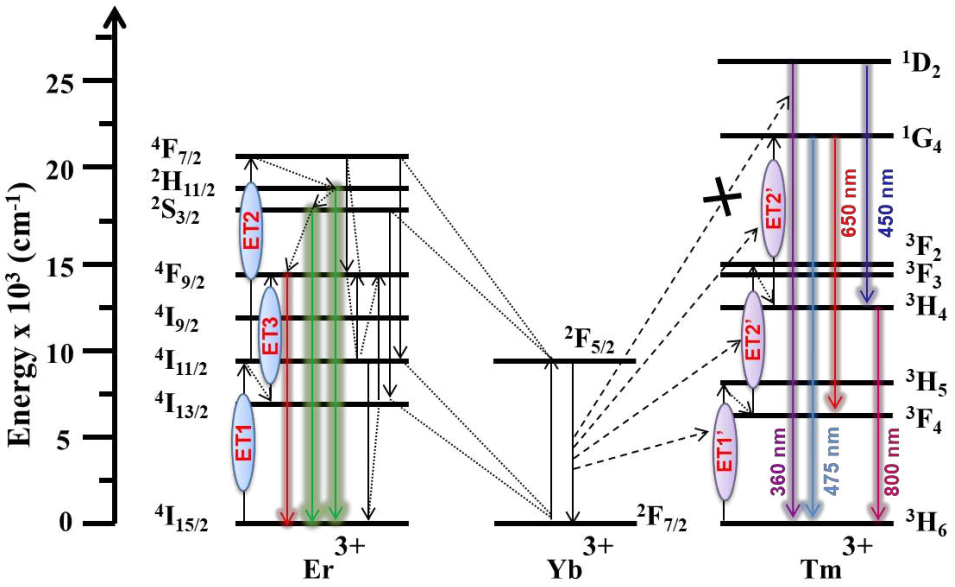

Fig. S5. Energy level diagrams showing the mechanism of electronic transitions in Fe^{3+} co-doped UCNP core.[2-3] Luminescence in lanthanides which mainly originates from f-f transitions are parity forbidden. However, as a result of mixing of ions with opposite parity, the selection rule is relaxed and therefore the probability of the electric dipole transitions is greatly increased as a consequence of asymmetric crystal field.[4] Doping of transition-metal ions, can lead to asymmetric crystal field, together with lanthanides in nanocrystals can effectively enhance the upconversion luminescence.[2, 4] As reported earlier, the doping of Fe^{3+} ions, because of its smaller ionic radius (0.60 °A) as compared to Y^{3+} (0.90 °A) shrinks the host lattice, thereby, alters the electronic environment around the activators (Er^{3+} and Tm^{3+}).[2, 4] This breaking of local symmetry results in relaxation of selection rules due to the creation of electric dipoles for which the transitions become allowed. Thus, overall enhancement of emission intensities is observed as a consequence of increasing probabilities of hypersensitive transitions in the crystal system. An Yb^{3+} ion is excited to the $^2F_{5/2}$ level by absorbing the NIR light. The Yb^{3+} ion, with excited state $^2F_{5/2}$, has comparable energy to $^4I_{11/2}$ (Er^{3+}), which in turn can sensitize Er^{3+} and transfer its energy to the Er^{3+} ion in its ground state, resulting an excited $^4I_{11/2}$ level of Er^{3+} (ET1). A successive energy-transfer from $^2F_{5/2}$ (Yb^{3+}) to an excited Er^{3+} ($^4I_{11/2}$) ion, in the next step, promotes the Er^{3+} ion to $^4F_{7/2}$ (ET2). The Er^{3+} ion is rapidly and non-radiatively relaxed from this state to the low lying $^2H_{11/2}$ and $^4S_{3/2}$ levels, producing two kinds closely ranged wavelengths of green (517 to 532 and 532 to 551 nm) emissions. Alternatively, red upconversion emission can occur either by non-radiative relaxation that can populate the $^4F_{9/2}$ state by its upper states $^2H_{11/2}$ + $^4S_{3/2}$ or through a separate mechanism involving $^4I_{11/2}$ (Er^{3+}) to $^4I_{13/2}$ (Er^{3+}) relaxation, which is then followed by an energy transfer

(ET3) from $^2F_{5/2}$ (Yb^{3+}) + $^4I_{13/2}$ (Er^{3+}) to $^2F_{7/2}$ (Yb^{3+}) + $^4F_{9/2}$ (Er^{3+}) level.[2] Furthermore, doping of Tm^{3+} into the core UCNP facilitated electronic transitions resulting intense emissions in UV, blue and NIR regions. The blue emission by a 3 photon process or a violet emission by 4 photon upconversion results from multiple energy resonances in the system. Additionally, the UV emission (at 360 nm, 4 photon process), blue emission (at 450 nm, 4 photon process) and NIR emission (at 800 nm) result from transition from $^1D_2$ to $^3H_6$, $^1D_2$ to $^3H_4$ and $^3H_4$ to $^3H_6$, respectively. Energy-transfer from Yb^{3+} to Tm^{3+} populates $^3H_5$ state of Tm^{3+} from $^3H_6$ (ET1'). The $^3H_5$ rapidly decays to $^3F_4$ level, which upon second energy transfer step (ET2') excites the Tm^{3+} from $^3F_4$ to $^3F_2$ that again decays rapidly to $^3H_4$ level. Also, a third transfer step (ET3') excites the Tm^{3+} from $^3H_4$ to $^1G_4$, which upon radiative relaxation back to $^3H_6$ yields a blue emission. A fourth energy transfer step from Yb^{3+} to Tm^{3+} could also occur to populate the Tm^{3+} ion from $^1G_4$ to $^1D_2$, however, due to large energy mismatch the chances for this transition is less likely. An alternative way through cross relaxation to populate $^1D_2$ the adjacent Tm^{3+} can happen through three possible routes: $^3F_2$ to $^3H_6$ and $^3H_4$ to $^1D_2$; $^1G_4$ to $^3F_4$ and $^3H_4$ to $^1D_2$; and $^1G_4$ to $^1D_2$ and $^3H_4$ to $^3F_4$. The relaxation of $^1D_2$ to $^3F_4$ leads to a violet emission.[3]

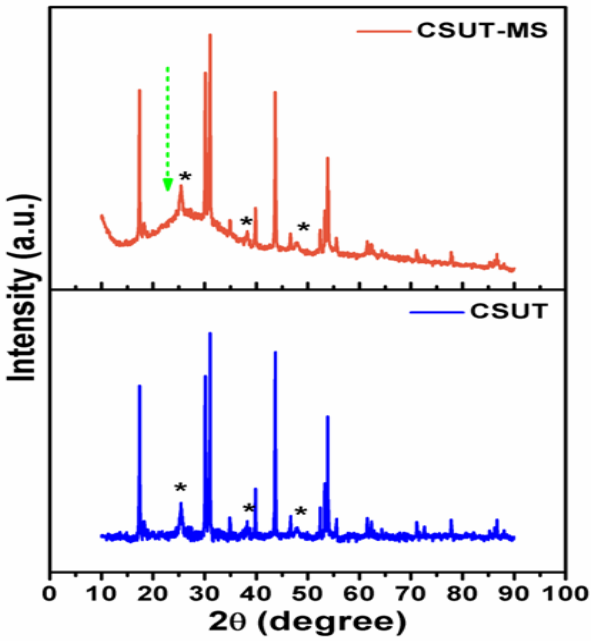

Fig. S6. Wide angle powder XRD of TiO_2 decorated CSU (CSUT) and mesoporous silica functionalized CSUT (CSUT-MS); the anatase titania peaks have been star marked. A broad peak due amorphous nature due to mesoporous silica layer shown with green arrow.

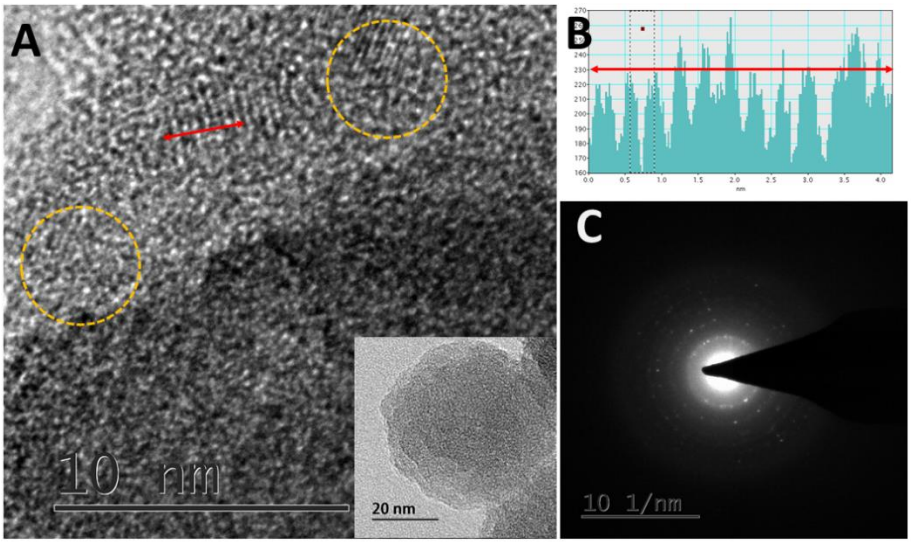

Fig. S7. (A) HRTEM image of titania decorated core-shell upconversion (CSUT) nanoparticles; titania nanoparticles are shown in yellow circles (CSUT in shown in inset under low magnification). (B) Lattice profile of titania nanoparticles, 0.33 nm (in the image double headed arrow marked) (C) SAED pattern from titania nanoparticles in CSUT.

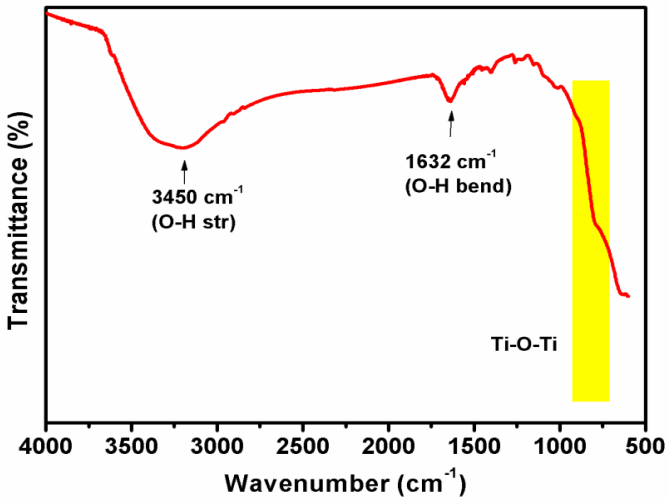

Fig. S8. FTIR spectrum of titania decorated core-shell upconversion (CSUT) nanoparticles. The strong absorption observed below 850 cm^{-1} was due to lattice vibrations of decorated TiO_2 NPs[5]. Furthermore, broad peak around 3450 cm^{-1} attributed to the O-H stretching and a band at 1632 cm^{-1} is assigned for the bending modes of O-H groups of adsorbed water molecules.

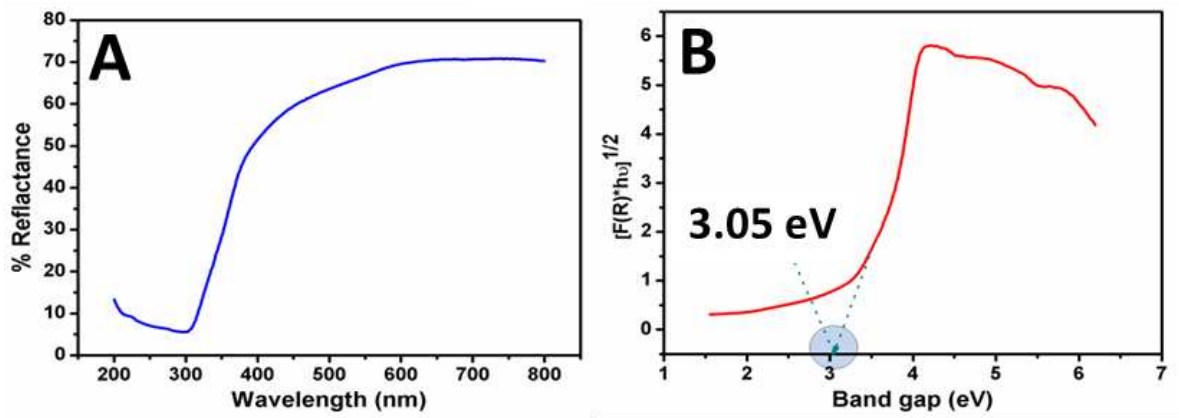

Fig. S9. (A) Solid UV-vis spectra of CSUT-MS. (B) Tauc's plot for band-gap calculation for CSUT-MS.

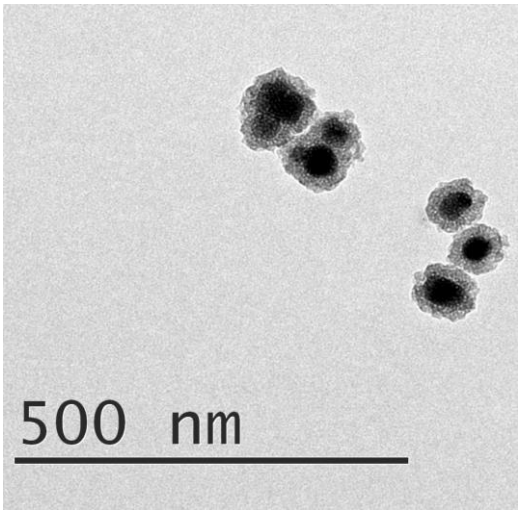

Fig.S10. TEM image of mesoporous silica (MS) layer coated titania decorated core-shell upconversion (CSUT) nanoparticles.

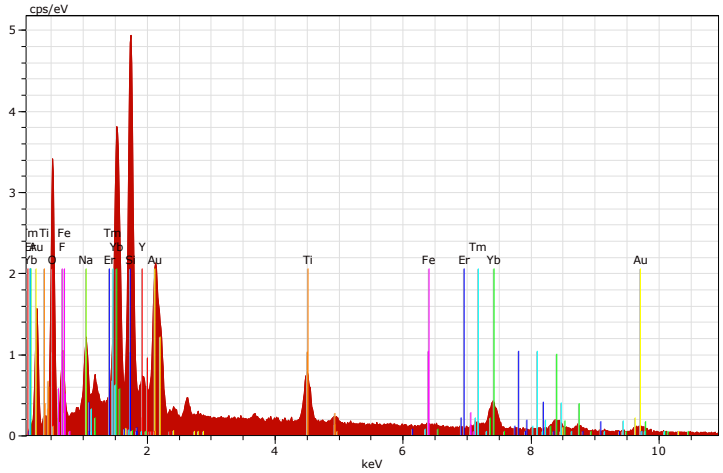

Fig. S11. The EDAX spectra of CSUT-MS showed the presence of Ti, Si and O along with the other constituents of CSU (from FESEM analysis).

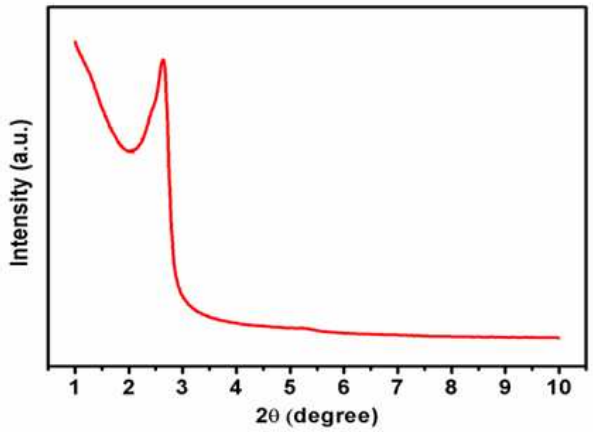

Fig. S12. Small angle powder XRD of CSUT-MS.

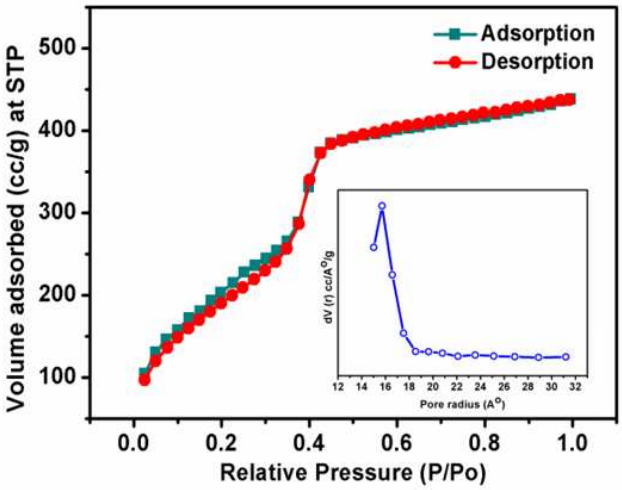

Fig. S13. N_2 sorption analysis and corresponding BJH pore size analysis (inset) showing MCM-41 behavior of CSUT-MS

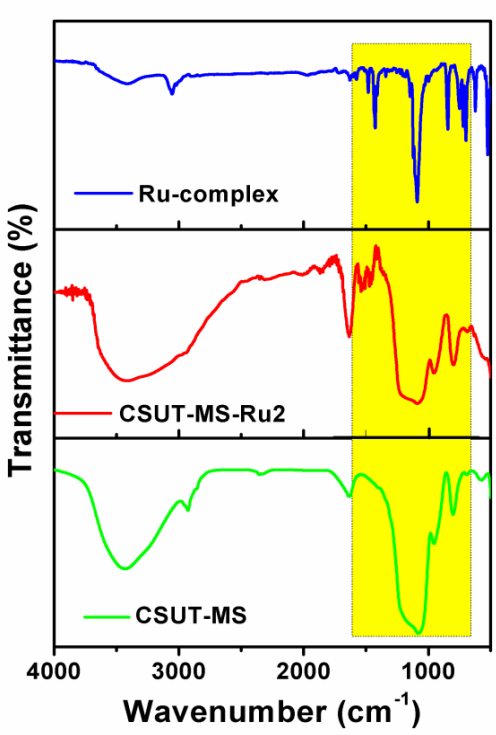

Fig. S14. FTIR analysis of free amino group containing CSUT-MS (green curve) and post conjugation with Ru-complex (Ru2) as gate-keeping molecules (red-curve), the spectrum free Ru2 molecules have been shown in blue curve

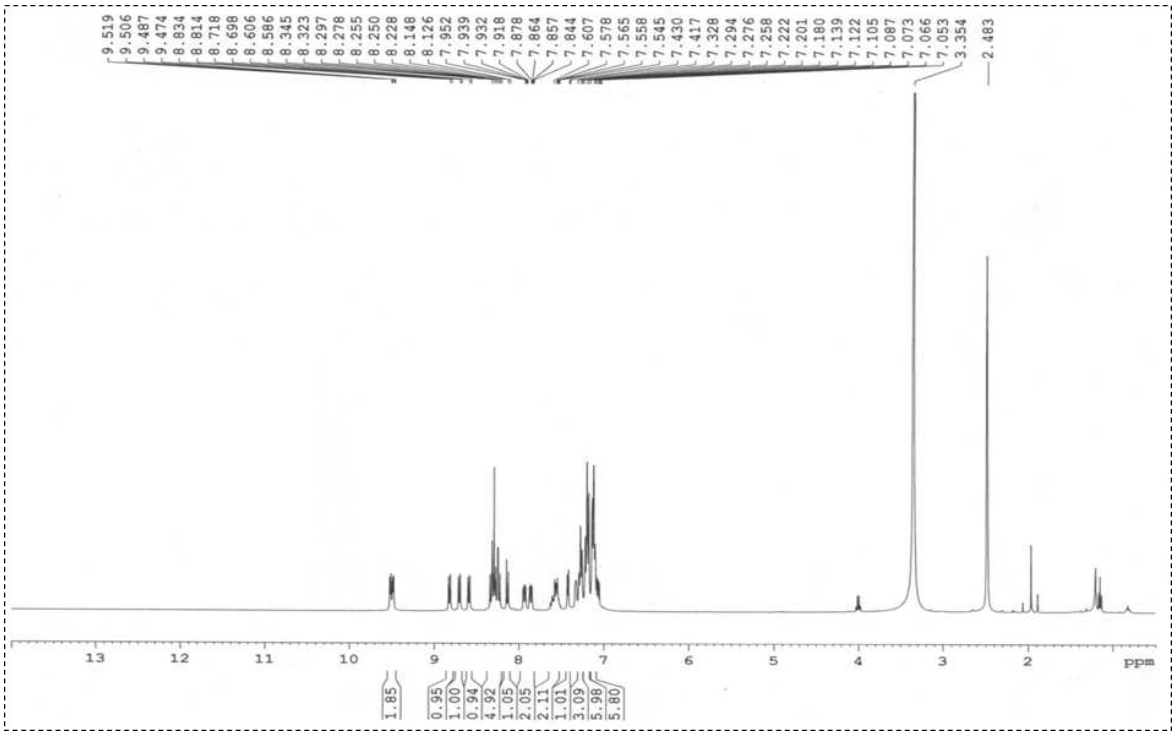

Fig.S15. ^{1}H-NMR spectrum of Ru(1,10-Phen)$_2$PPh$_3$Cl complex (Ru2).

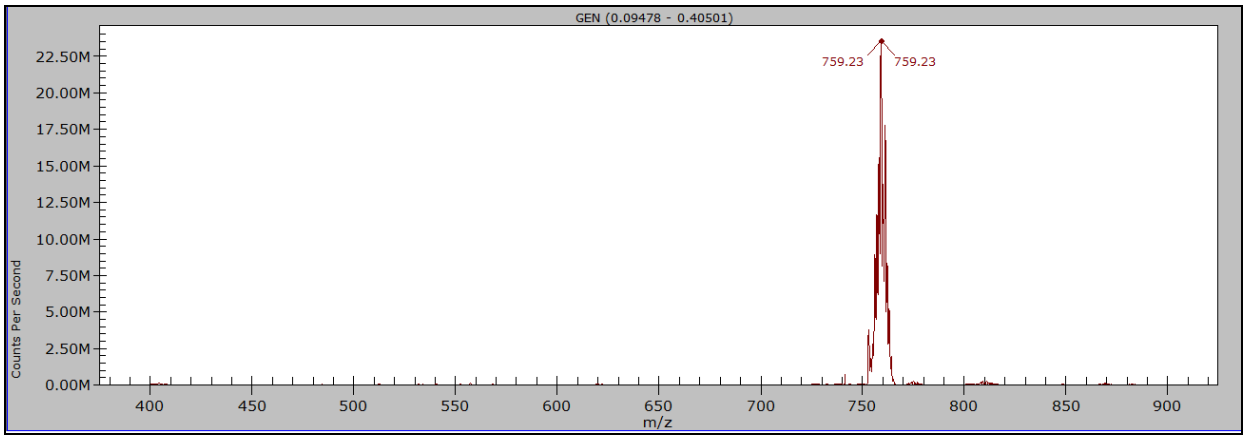

Fig. S16. ESI-MS analysis Ru-complex showed a % [M^+] ion peak for the complex at m/z 759.23, corresponding to the molecular weight of the as-prepared $Ru(1,10\text{-}Phen)_2PPh_3Cl$.

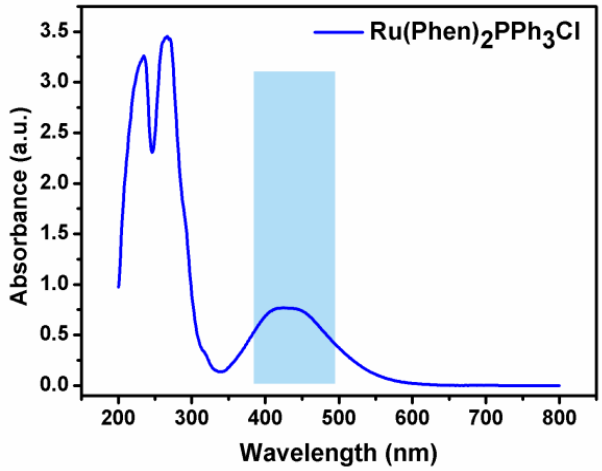

Fig. S17. UV-vis analysis of Ru-complex (Ru2).

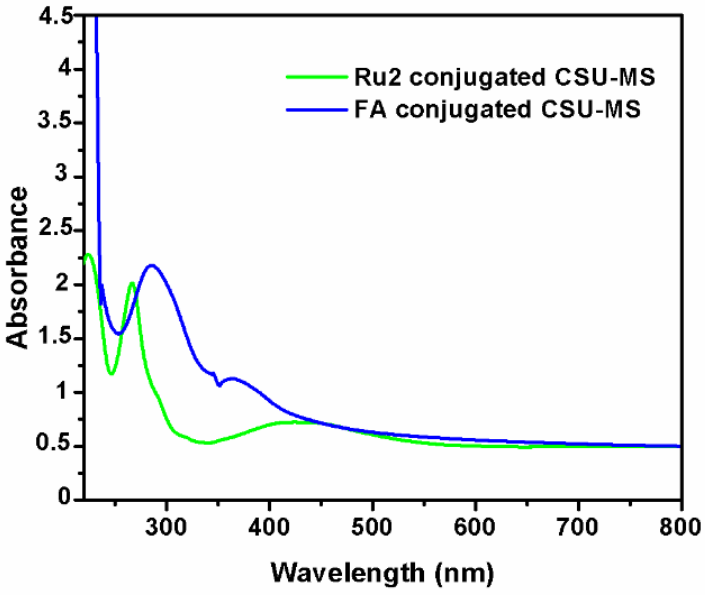

Fig. S18. UV-vis analysis of Ru2 conjugated (green curve) and folic acid (FA) conjugated CSU-MS (blue curve). the Ru-complex bound CSU-MS showed a broad band at 360-480 nm (approx.), which was attributed to metal-to-ligand charge transfer (MLCT) band of the Ru complex. Additionally, the band at 290 nm is assigned to π-π* transition of the phenanthroline ligand in the Ru complex. The attachment of FA to amine functionalized CSU-MS resulted in appearance of absorbance maxima around 285 nm due to pterin ring in FA.

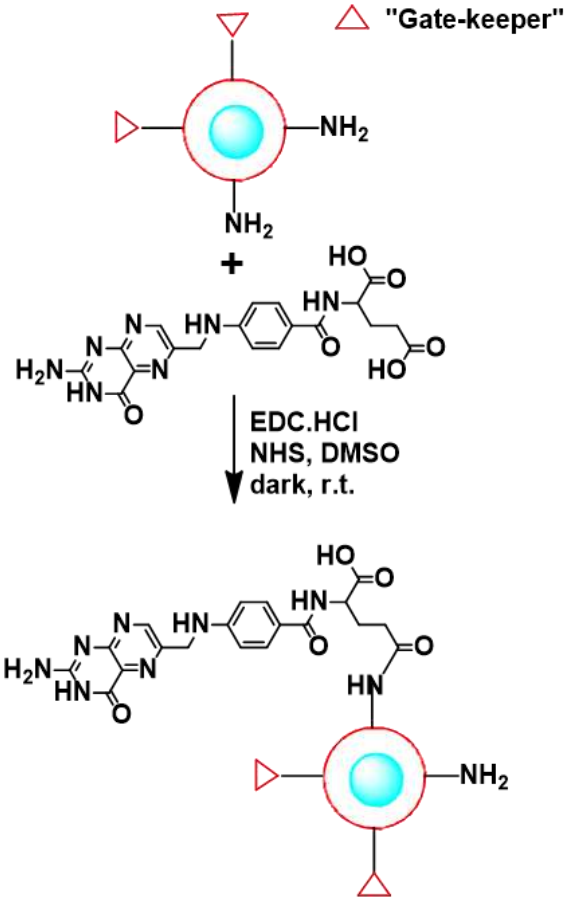

Fig. S19. The chemical reaction involving conjugation of FA to CSUT-MS via EDC coupling.

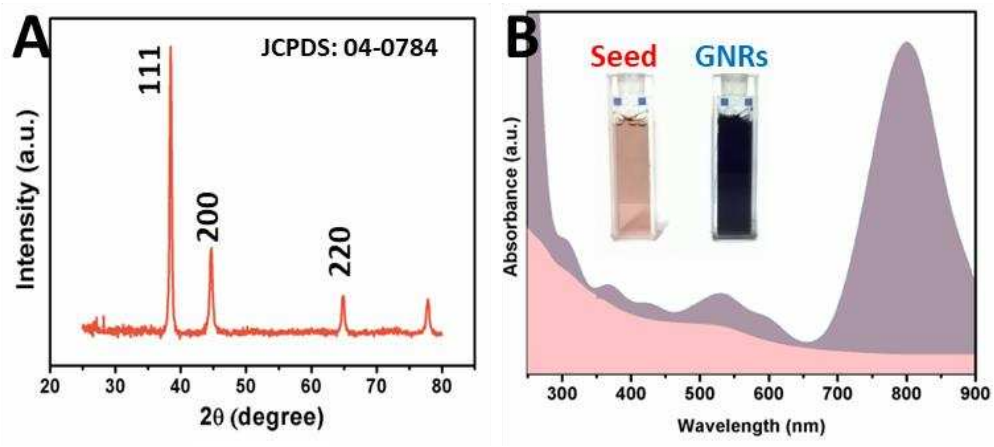

Fig. S20. (A) XRD analysis of as synthesised GNRs. (B) UV-vis-NIR analysis of seed (light pink curve) and GNRs (light purple curve); the corresponding seed solution (light brown) and GNR solution (dark blue) (inset).

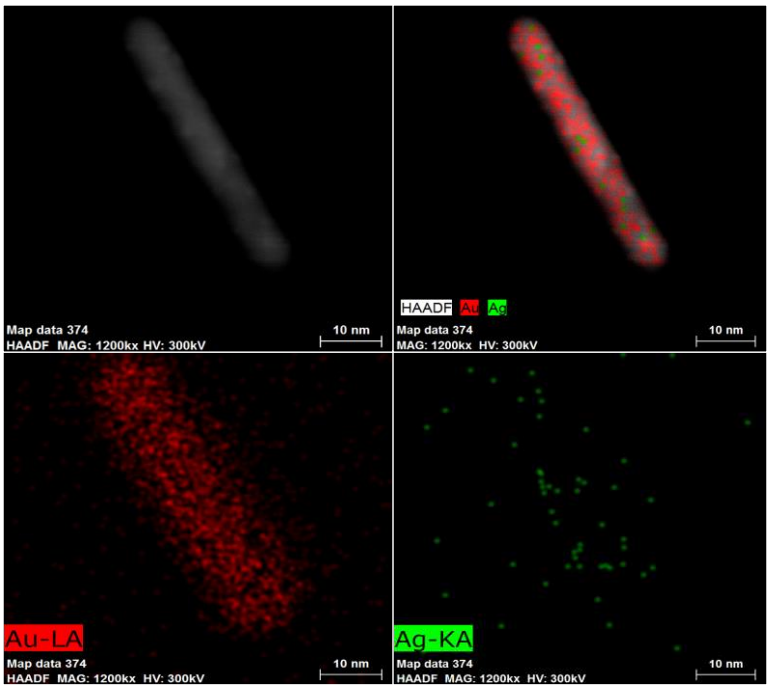

Fig. S21. EDAX analysis for elemental mapping of as-synthesized GNRs.

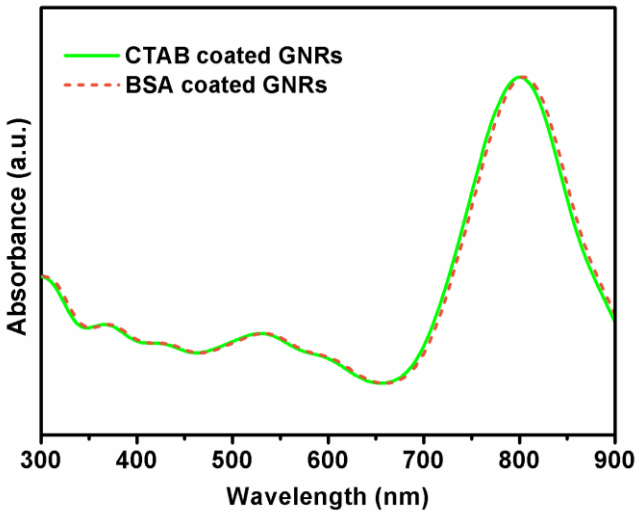

Fig. S22. The UV-vis-NIR studies showed that BSA coating did not affect the absorbance maxima of the GNRs. A small shift in LSPR was observed due to the probable change in the refractive index of the GNRs surface owing to the coating of BSA.

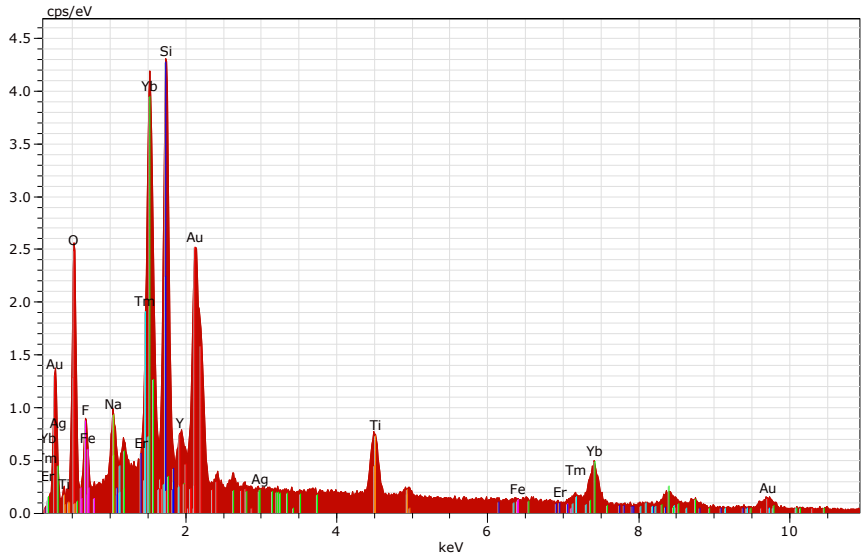

Fig. S23. The EDAX analysis of GNR decorated CSUT-MS was further evidenced by the presence of Au and Ag in the spectrum along with the other constituents of CSUT-MS

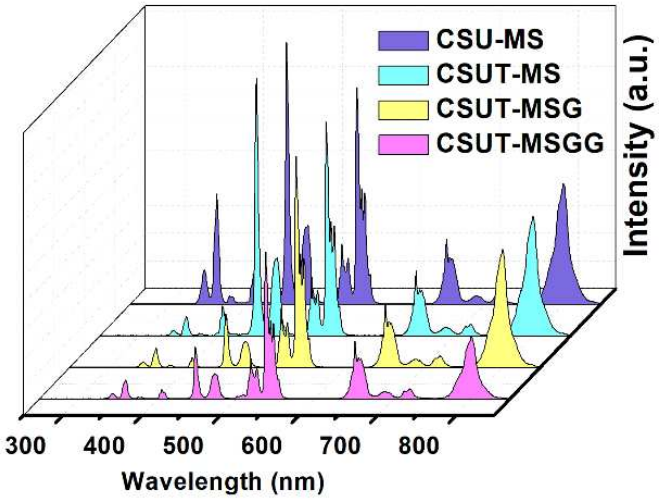

Fig. S24. Steady-state fluorescence analysis after each modification step clearly showed quenching of UC emission in UV, blue and in NIR (800 nm) regions as a result of the modifications in the nanoplatform with the integrated photoactive agents, i.e., TiO_2, Ru-complex and GNRs, in CSUT-MS, CSUT-MSG and CSUT-MSGG, respectively, establishing the energy transfer phenomenon.

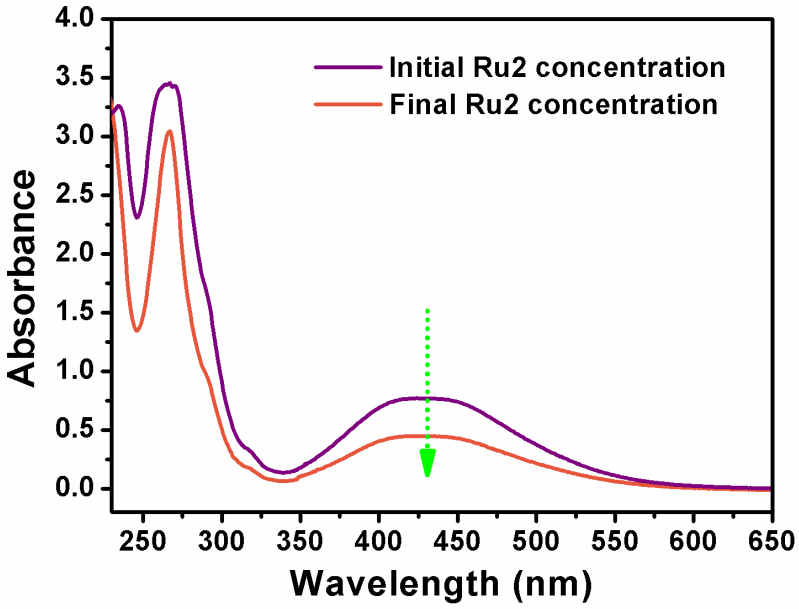

Fig. S25. Loading studies of Ru2 by UV-Vis analysis.

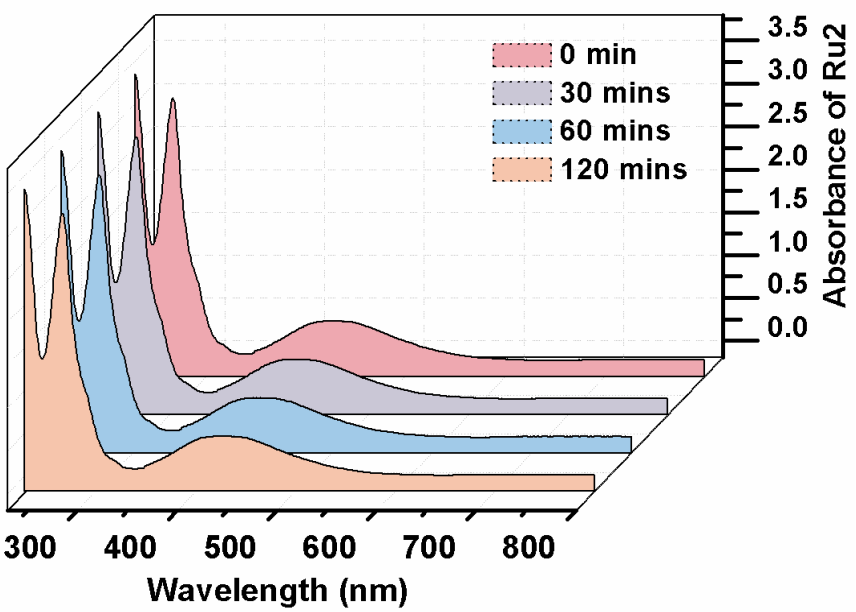

Fig. S26. In the absence of blue light, NIR exposure of Ru-complex without the upconversion nanoparticles does not show any red-shift even after 120 mins of irradiation.

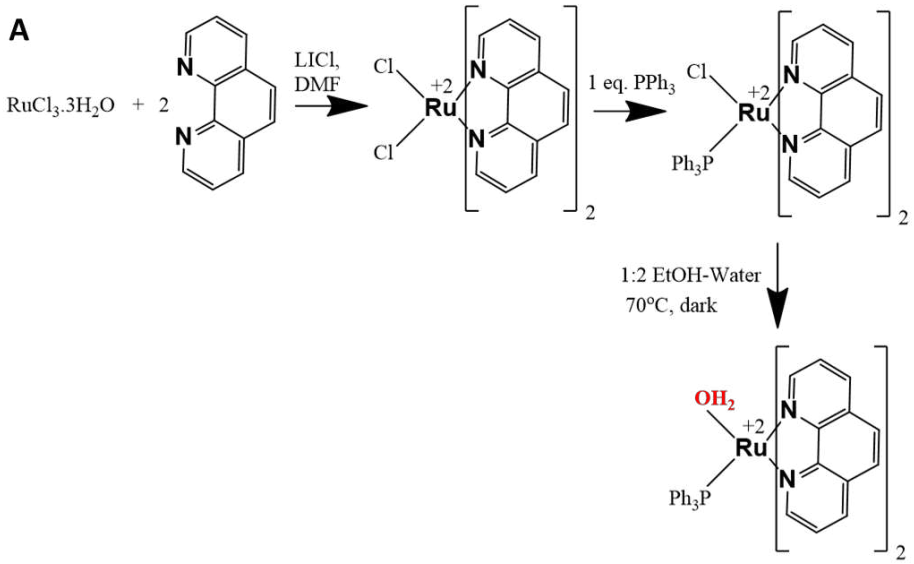

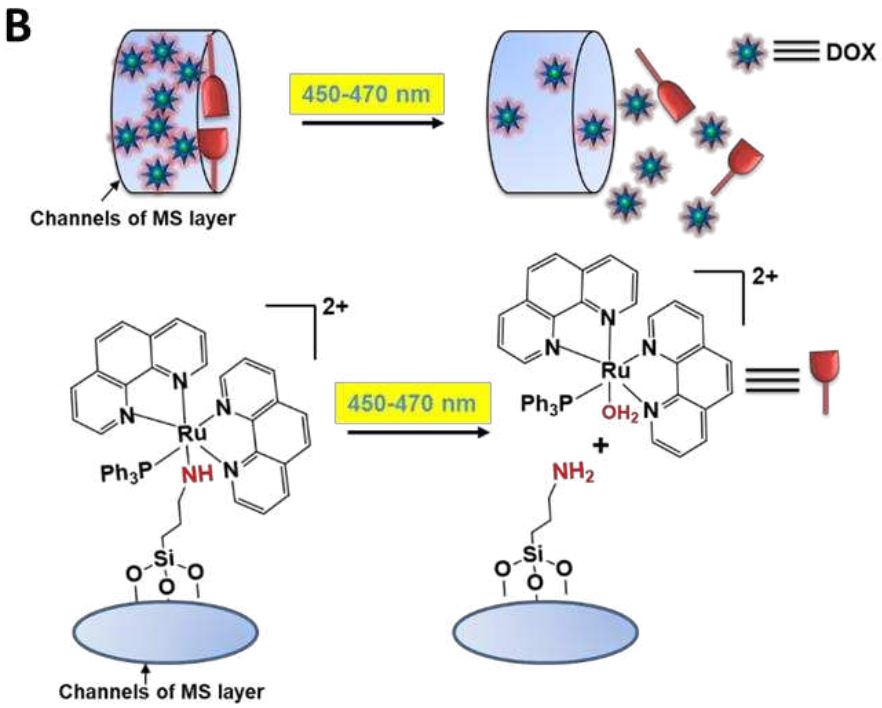

Fig. S27. A) Synthetic route for Ru-complex. B) schematic representation of DOX release from the nanoplatform in response to the cleavage of Ru-complex by blue emission from CSU.

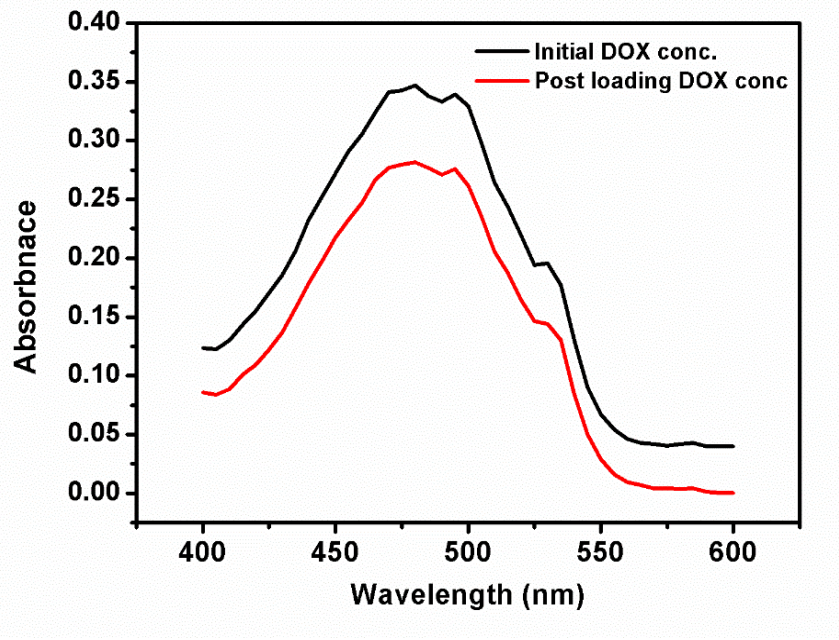

Fig. S28. Doxorubicin (DOX) loading analysis through UV-vis spectroscopy. The DOX loading % was calculated to be 17% (approx.), *i.e.*, 0.51 mg/ 30 mg of nanoplatform taken for loading.

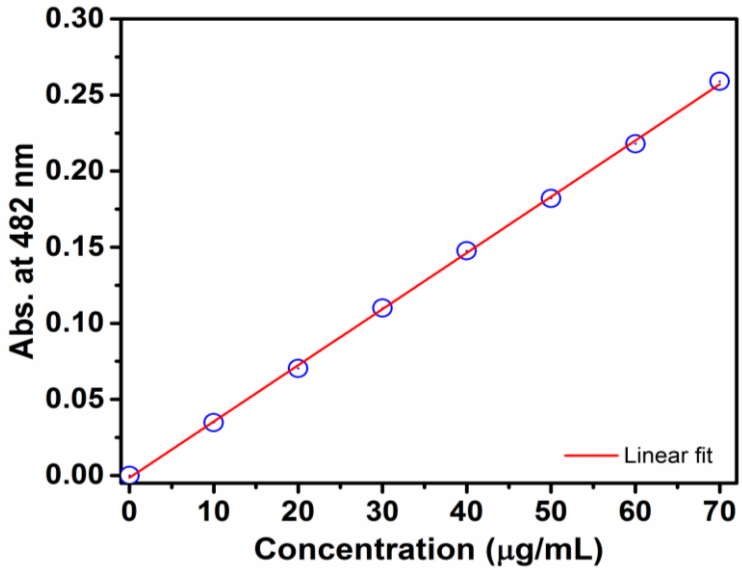

Fig. S29. Standard curve for Doxorubicin (DOX).

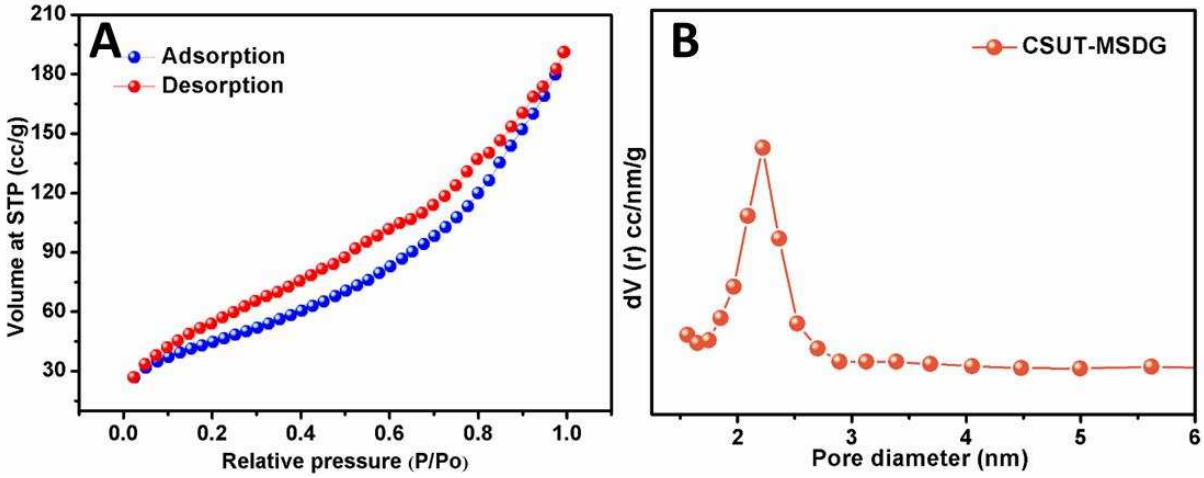

Fig. S30. (A) N_2-sorption isotherm and corresponding (B) BJH pore-size distribution after DOX and Ru-conjugation to CSUT-MS.

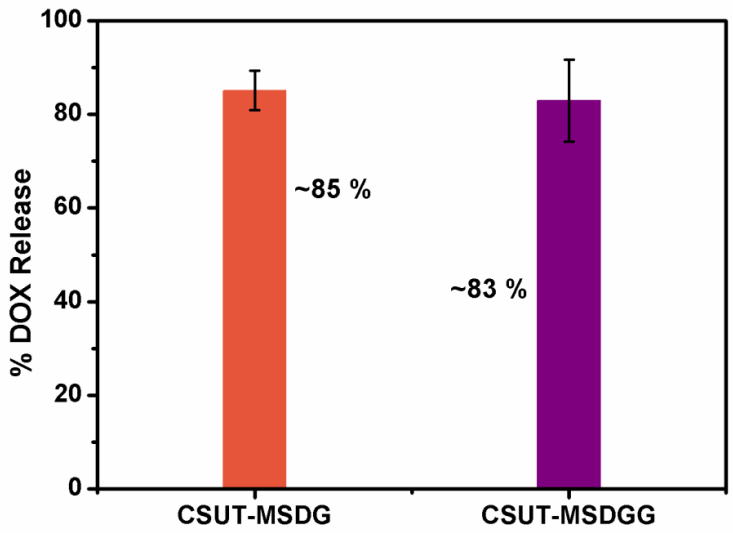

Fig. S31. DOX release from CSUT-MSDG showed no significance difference (approx. 85 %) as compared to CSUT-MSDGG, indicating heating did not affect the DOX release.

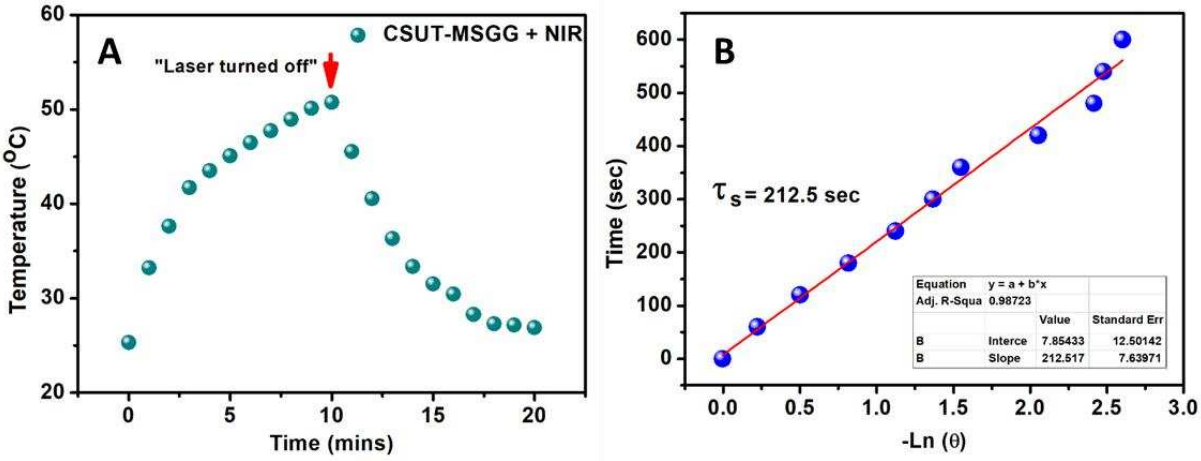

Fig. S32. Heating/Cooling experiment of 200 μg/mL GNR decorated nanoplatform in response to the NIR laser exposure (A) The laser was switched off after 10 min of heating period and the cooling rate was recorded. (B) Plot of cooling response after the NIR laser was turned off, T(sec) *vs.* –Ln(θ). The photothermal conversion efficiency (η) of the GNR decorated nanoplatform was determined by the method reported earlier.[6] The photothermal conversion efficiency (η) is given by following equation:

$$\eta = \frac{hS\,(T_{max} - T_{surr}) - Q_{dis}}{I\,(1 - 10^{-A_{800}})} \qquad \text{i}$$

$$\text{Where,} \qquad hS = \frac{(m_D C_D)}{\tau_s} \qquad \text{ii}$$

$$\text{And,} \qquad \tau_s = -Ln(\theta) \qquad \text{iii}$$

Further,

$$\theta = \frac{(T(t) - T_{surr})}{(T_{max} - T_{surr})} \qquad \text{iv}$$

h is the heat transfer co-efficient, *S* is the surface area of the container. The maximum temperature (T_{max}) of the solution containing the nanoplatform after laser irradiation was 50.6 ºC and surrounding temperature (T_{surr}) was 25.5 ºC. The temperature change (T_{max}-T_{surr}) of the solution was calculated as 25.1 ºC. In addition, *m* is 0.2 g and *C* is 4.2 J/g ºC. Thus, using eq. iv, *hS* can be calculated as 3.87 mW/ºC. The laser power *I* is 0.280 W at 980 nm. The absorbance (A_{800}) or optical density of GNR decorated nanoplatform dispersion at 800 nm is 0.91. Q_{dis} was measured independently to be 0.030 W using a quartz cuvette cell containing pure water. It expresses the heat dissipated from the light absorbed by the solvent and quartz sample cell itself. A half-life time constant (τ_s) can be calculated from the cooling phase after the laser was turned-off. Using eq. iii, a linear plot between T(sec) *vs.* –Ln(θ), the value of τ_s was given by the slope of the linear fit as 212.5 sec. Finally, after substituting all the values for corresponding parameters in eq. i, the photothermal conversion efficiency (η) is calculated as 20.8%, similar to the GNR based thermal therapies reported earlier.[7-8]

A	DI water Size (nm)		PBS Size (nm)		DMEM Size (nm)	
	Fresh dispersion	After 6 h	Fresh dispersion	After 6 h	Fresh dispersion	After 6 h
CSUT	68.1 ± 3.4	164 ± 2.1	78.8 ± 5.2	186 ± 2.8	106.3 ± 1.3	291 ± 3.2
CSUT-MS	91.3 ± 1.4	190 ± 3.1	88.8 ± 7.4	220 ± 5.1	94.3 ± 2.5	220 ± 3.8
CSUT-MSDG	142 ± 2.3	255 ± 4.4	122 ± 6.2	164 ± 8.5	142 ± 3.7	342 ± 7.0
CSUT-MSDGG	164 ± 1.8	531 ± 5.6	189 ± 3.0	615 ± 1.9	218 ± 6.6	825 ± 8.1

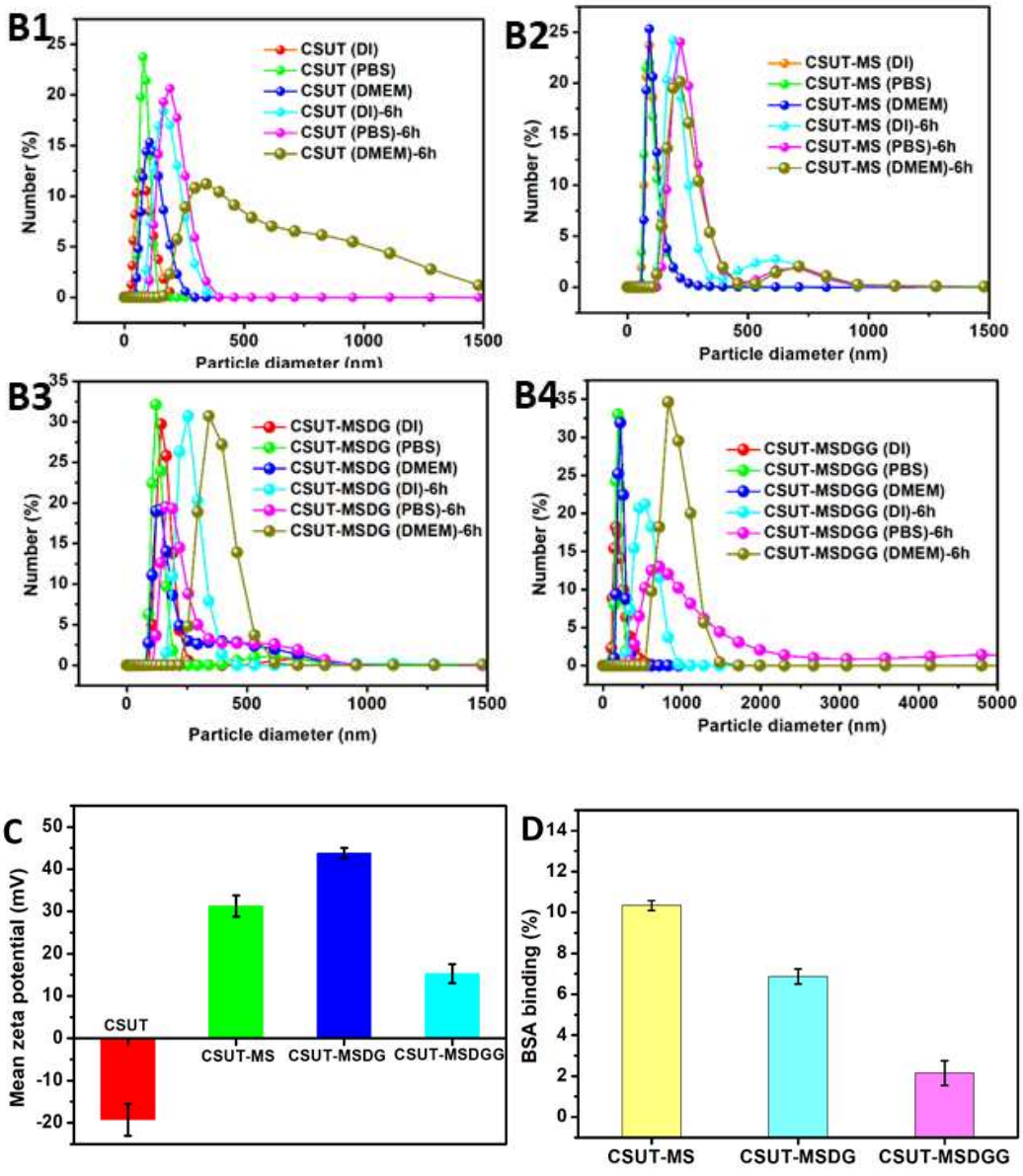

Fig. S33. Characterizations in biological media: (A) Table showing diameter of the particles in different dispersion medium (DI water, PBS buffer and DMEM media with 10 % FBS) in freshly prepared conditions and when left undisturbed after 6 h. (B) The corresponding DLS graphs have been depicted showing the size distribution of the nanoparticles, *i.e.,* CSUT,

CSUT-MS, CSUT-MSDG and CSUTMSDGG, in different media prepared in the conditions mentioned before. (C) Zeta-potential analysis of CSUT, CSUT-MS, CSUT-MSDG and CSUT-MSDGG was observed as -19.3 ± 3.8 mV, 31.3 ± 2.5 mV, 43.8 ± 1.2 mV and 15.3 ± 2.2 mV respectively. (D) Protein binding assay. From the DLS results it can be observed that the freshly dispersed particles showed slight increase in the diameter in high salt concentration conditions (PBS buffer) and in DMEM media (with 10 % FBS) as compared to the ion free (DI water) conditions. This trend was consistent for all the particle sets. The increase in size for both, the freshly prepared dispersion and the 6 h old dispersion (the DLS measurement of 6 h old dispersion was recorded after a gentle tap) in DMEM media can be attributed the interactions of nanoparticles with the media components. Zeta potential of the nanoplatform being an important parameter determines the particles behavior to interact with the serum proteins, in turn, with the targeted cellular surface. Also, the fact that, a zeta potential in the range of -10 to +10 mV can still be considered neutral,[9] and nanoparticles with near neutral surface charge can effectively avoid interaction with serum protein, thereby, can circumvent their clearance by reticuloendothelial system (RES). This neutral or near neutral surface property would be at an advantage over the nanoparticles with high charge on their surface. In this context, our final system, CSUT-MSDGG (zeta: +15.3 ± 2.25 mV), demonstrates required chemical features favourable for the cellular interactions. Next, protein-binding assay was carried out to mimic the serum proteins in the biologically environment. Strictly speaking, the interaction of the nanoparticles with serum protein helps removing the particles from the biological environment by RES system. In this regard, a nanoformulation, by virtue of its chemical behaviour, if it can minimize its interaction with the serum proteins, would be deemed suitable for the biological applications.[10] Herein, the protein binding assay clearly showed that our final system, CSUT-MSDGG, showed a BSA loading value of 4.3 μg/mg (2.1 % w.r.t. initial loading concentration), lower than in case of CSUT-MS and CSUT-MSDG. The low loading for the final systems, CSUT-MSDGG, can be

attributed to the extensive modifications that leads to unavailability of the particle surface and the channels to the protein molecules. These results clearly indicated that the fabricated nanocomposite exhibited favourable attributes to be applicable in biological system.

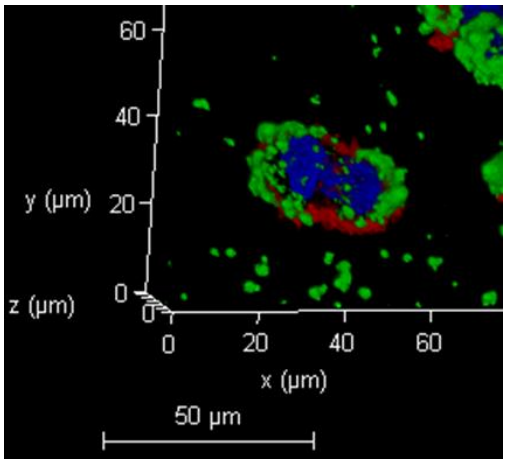

Fig. S34. Confocal analysis showing the nanoplatform without folic acid (FA) conjugation did not show appreciable uptake by HeLa cells and the particles were mostly found on the cells surface.

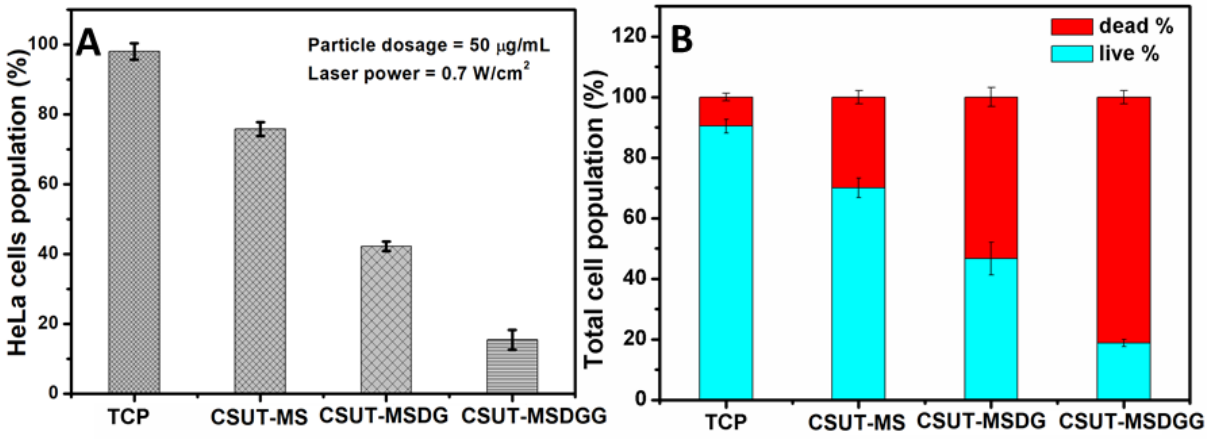

Fig. S35. (A) MTT assay upon NIR treatment. (B) Live-dead analysis on HeLa cells by Trypan blue dye exclusion assay. A dosage concentration of 50 µg/ml and 0.7 W/cm^2 NIR irradiation power was used for the studies.

References

1. Pan, L.; He, Q.; Liu, J.; Chen, Y.; Ma, M.; Zhang, L.; Shi, J., Nuclear-Targeted Drug Delivery of Tat Peptide-Conjugated Monodisperse Mesoporous Silica Nanoparticles. *J Am Chem Soc* **2012,** *134*, 5722-5725.
2. Ramasamy, P.; Chandra, P.; Rhee, S. W.; Kim, J., Enhanced Upconversion Luminescence in $NaGdF_4$:Yb,Er Nanocrystals by Fe^{3+} Doping and their Application in Bioimaging. *Nanoscale* **2013,** *5*, 8711-8717.
3. Yin, A.; Zhang, Y.; Sun, L.; Yan, C., Colloidal Synthesis and Blue Based Multicolor Upconversion Emissions of Size and Composition Controlled Monodisperse Hexagonal $NaYF_4$: Yb,Tm Nanocrystals. *Nanoscale* **2010,** *2*, 953-959.
4. Han, S.; Deng, R.; Xie, X.; Liu, X., Enhancing Luminescence in Lanthanide-Doped Upconversion Nanoparticles. *Angew. Chem. Int. Ed.* **2014,** *53*, 11702 - 11715.
5. Kumar, P. M.; Badrinarayanan, S.; Sastry, M., Nanocrystalline TiO_2 Studied by Optical, FTIR and X-Ray Photoelectron Spectroscopy: Correlation to Presence of Surface States. *Thin Solid Films* **2000,** *358* (1-2), 122-130.
6. Roper, D. K.; Ahn, W.; Hoepfner, M., Microscale Heat Transfer Transduced by Surface Plasmon Resonant Gold Nanoparticles. *J. Phys. Chem. C* **2007,** *111*, 3636-3641.
7. Li, Z.; Huang, H.; Tang, S.; Li, Y.; Yu, X.-F.; Wang, H.; Li, P.; Sun, Z.; Zhang, H.; Liu, C., Small Gold Nanorods Laden Macrophages for Enhanced Tumor Coverage in Photothermal Therapy. *Biomaterials* **2016,** *74*, 144-154.
8. Wang, B.; Wang, J.-H.; Liu, Q.; Huang, H.; Chen, M.; Li, K.; Li, C.; Yu, X.-F.; Chu, P. K., Rose-Bengal-Conjugated Gold Nanorods for In Vivo Photodynamic and Photothermal Oral Cancer Therapies. *Biomaterials* **2014,** *35*, 1954-1966.
9. Clogston, J. D.; Patri, A. K., Zeta Potential Measurement. In *Characterization of nanoparticles intended for drug delivery*, Springer: 2011; pp 63-70.
10. Chauhan, V. P.; Jain, R. K., Strategies for Advancing Cancer Nanomedicine. *Nat. Mater.* **2013,** *12*, 958-962.